AUTHOR(S):

Togo, Masaya; Matsumoto, Riki; Usami, Kiyohide; Kobayashi, Katsuya; Takeyama, Hirofumi; Nakae, Takuro; Shimotake, Akihiro; ... Miyamoto, Susumu; Takahashi, Ryosuke; Ikeda, Akio

Contents lists available at ScienceDirect

NeuroImage

journal homepage: www.elsevier.com/locate/neuroimage

Distinct connectivity patterns in human medial parietal cortices: Evidence from standardized connectivity map using cortico-cortical evoked potential

Masaya Togo [a,b], Riki Matsumoto [a,b,*], Kiyohide Usami [a], Katsuya Kobayashi [a], Hirofumi Takeyama [c,d], Takuro Nakae [e], Akihiro Shimotake [a], Takayuki Kikuchi [f], Kazumichi Yoshida [f], Masao Matsuhashi [g], Takeharu Kunieda [h], Susumu Miyamoto [f], Ryosuke Takahashi [a], Akio Ikeda [g,**]

[a] Department of Neurology, Kyoto University Graduate School of Medicine, Japan
[b] Division of Neurology, Kobe University Graduate School of Medicine, 7-5-2 Kusunoki-cho, Chuo-ku, Kobe, 650-0017, Japan
[c] Department of Respiratory Care and Sleep Control Medicine, Kyoto University Graduate School of Medicine, Japan
[d] Department of Neurology, Japanese Red Cross Otsu Hospital, Japan
[e] Department of Neurosurgery, Shiga General Hospital, Japan
[f] Department of Neurosurgery, Kyoto University Graduate School of Medicine, Japan
[g] Departments of Epilepsy, Movement Disorders and Physiology, Kyoto University Graduate School of Medicine, 54 Kawahara-cho, Sakyo-ku, Kyoto, 606-8507, Japan
[h] Department of Neurosurgery, Ehime University Graduate School of Medicine, Japan

ARTICLE INFO

ABSTRACT

The medial parietal cortices are components of the default mode network (DMN), which are active in the resting state. The medial parietal cortices include the precuneus and the dorsal posterior cingulate cortex (dPCC). Few studies have mentioned differences in the connectivity in the medial parietal cortices, and these differences have not yet been precisely elucidated. Electrophysiological connectivity is essential for understanding cortical function or functional differences. Since little is known about electrophysiological connections from the medial parietal cortices in humans, we evaluated distinct connectivity patterns in the medial parietal cortices by constructing a standardized connectivity map using cortico-cortical evoked potential (CCEP). This study included nine patients with partial epilepsy or a brain tumor who underwent chronic intracranial electrode placement covering the medial parietal cortices. Single-pulse electrical stimuli were delivered to the medial parietal cortices (38 pairs of electrodes). Responses were standardized using the z-score of the baseline activity, and a response density map was constructed in the Montreal Neurological Institutes (MNI) space. The precuneus tended to connect with the inferior parietal lobule (IPL), the occipital cortex, superior parietal lobule (SPL), and the dorsal premotor area (PMd) (the four most active regions, in descending order), while the dPCC tended to connect to the middle cingulate cortex, SPL, precuneus, and IPL. The connectivity pattern differs significantly between the precuneus and dPCC stimulation ($p<0.05$). Regarding each part of the medial parietal cortices, the distributions of parts of CCEP responses resembled those of the functional connectivity database. Based on how the dPCC was connected to the medial frontal area, SPL, and IPL, its connectivity pattern could not be explained by DMN alone, but suggested a mixture of DMN and the frontoparietal cognitive network. These findings improve our understanding of the connectivity profile within the medial parietal cortices. The electrophysiological connectivity is the basis of propagation of electrical activities in patients with epilepsy. In addition, it helps us to better understand the epileptic network arising from the medial parietal cortices.

1. Introduction

The medial parietal cortices, especially the precuneus and the dorsal posterior cingulate cortex (dPCC), are associated with a variety of functions, including visuospatial imagery, episodic memory retrieval, and self-processing (Cavanna and Trimble, 2006), recognition of places (Sugiura et al., 2005). Impairments of these areas result in topographical disorientation (Takahashi et al., 1997). These areas are also components of the default mode network (DMN) that is active both during the resting state (Fransson and Marrelec, 2008; Raichle, 2015; Raichle et al., 2001) and various internally directed cognitions, such as introspective processes (Andrews-Hanna et al., 2014; Dixon et al., 2018) or self-reported mind-wandering (Christoff et al., 2016; Fox et al., 2018). Other than internally directed cognition, the precuneus also seems to play a pivotal role in motor-related functions such as visual guided hand movements (Caminiti et al., 1999; Cavanna and Trimble, 2006). Direct recordings from the posteromedial cortex have revealed functional differentiation within the region (Daitch and Parvizi, 2018). Although such heterogenicity of the human medial parietal cortices have been reported, the differences in connectivity within the network have not yet been entirely clarified.

A precise definition of inter-cortical connectivity is essential to understanding the complex functional organization of various brain functions. Anatomical connections of the medial parietal cortices have been assessed by using invasive tracers in macaque monkeys (Parvizi et al., 2006; Passarelli et al., 2011; Pandya et al., 1981; Vogt and Pandya, 1987), and functional connectivity or cytology in humans (Bzdok et al., 2015; Cauda et al., 2010; Hutchison et al., 2015; Margulies et al., 2009; Vogt et al., 2006; Yu et al., 2011; Zhang and Li, 2012; Zhang et al., 2014). These studies have proposed various types of connections or parcellations of the medial parietal cortices, dPCC, and precuneus. Some studies investigated only one of these two regions or the precuneus was not parcellated into subdivision. The precise difference in connectivity within the medal parietal cortices has not yet been clarified.

Effective connectivity, defined as the influence that one neural system exerts over another, either at a synaptic or population level (Friston, 2011), is an approach that takes advantage of the causal relationship between two brain areas, in contrast to structural or functional connectivity (Arbune et al., 2020). Cortico-cortical evoked potential (CCEP) is a method to electrophysiologically assess direct and effective cortico-cortical connectivity by applying single-pulse electrical stimulation to cerebral cortices. The CCEP responses recorded from the remote cortical areas with latencies under 50 ms (N1 activity) are supposed to represent the direct orthodromic propagation through the cortico-cortical connections (Keller et al., 2014b; Matsumoto et al., 2017, 2004). The strength of the activity assumed from CCEP amplitudes is positively correlated with the white matter tract quantity as measured with diffusion tensor imaging (DTI) (Conner et al., 2011; Keller et al., 2014b). In addition, the connectivity pattern of CCEP has been reported to be similar to that of resting-state functional connectivity (Keller et al., 2011, 2014a; Nakae et al., 2020).

Electrophysiological connectivity of the lateral ventral parieto-frontal network has already been investigated (Matsumoto et al., 2012). However, electrophysiological connections from medial parietal cortices to the other cortices have not been well studied, although the medial parietal cortices are often targeted by resting-state functional MRI (fMRI) research studies. This is partially due to the rarity and difficulty of precisely implanting subdural grid electrodes in the medial parts of the cerebral cortex. Several studies have investigated cortico-cortical evoked potentials using intracranial electrodes, mainly stereotactic electroencephalography (SEEG), to stimulate the posterior cingulate gyrus or the precuneus (Enatsu et al., 2014, 2015; Keller et al., 2014; Parvizi et al., 2021). However, in SEEG, depth electrodes are inserted sparsely (each electrode is ~3 cm apart), making it technically difficult to study the detailed connections two-dimensionally in detail from the medial surface of the parietal cortices. We therefore mainly focused on subdural grid recording in the present study, since we can probe the connections from the medial parietal surface to other cortices more densely, namely, at a spatial resolution reflecting the inter-electrode distance (1 cm).

Herein, to clarify the distinct connectivity patterns within the medial parietal cortices, we attempted to elucidate the parcellation in the medial parietal cortices based on the electrophysiological connectivity using standardized CCEP data. We also made a connectivity map surrounding the medial parietal cortices, namely the paracentral lobule (PCL) and superior parietal lobule (SPL), for comparison. In addition, we verified the CCEP connectivity results against those obtained from the resting-state functional connectivity open database.

2. Methods

2.1. Patients

We recruited nine patients with partial epilepsy, including six with focal cortical dysplasia and the remaining three with brain tumors. They underwent chronic intracranial electrode placement covering the superior or medial parietal cortices for the presurgical evaluation. The clinical profiles of the investigated patients are presented in Table 1.

The implanted electrodes were made of platinum measuring 2.3 mm (Ad-Tech, Racine, WI) in diameter with a center-to-center interelectrode distance of 1 cm. In patient 9, stereotactic electroencephalography (SEEG) implantation was performed using multi-lead depth electrodes (AdTech, Racine, WI). Although the stimulation parameters or limits need to be adapted, CCEPs can be evaluated in SEEG, as is done in subdural recording with electrocorticograms (ECoGs) (Prime et al., 2018; Trebaul et al., 2018). The electrodes were implanted according to the Talairach stereotactic method using orthogonal or oblique trajectories. The present study was approved by the Ethics Committee of Kyoto University Graduate School of Medicine (IRB No. 443/C1212). Informed consent was obtained from all patients. This work abides by the central tenets of the Declaration of Helsinki.

2.2. Anatomical location of electrodes

To define the precise location of each electrode on the surface of the brain, subdural electrodes were coregistered to three-dimensional volume-rendered MRIs, which were reconstructed from magnetization-prepared rapid gradient-echo (MP-RAGE) sequences. The location of each electrode was identified on the 2D MRIs using its signal void due to the property of the platinum alloy. Electrodes locations were non-linearly co-registered to the patient MP-RAGE taken before implantation, and then to MNI standard space using FLIRT (FMRIB's Linear Image Registration Tool) and FNIRT (FMRIB's Non-linear Image Registration Tool) (https://fsl.fmrib.ox.ac.uk/fsl/fslwiki) (Matsumoto et al., 2004; Matsumoto et al., 2011). in all patients but Patient 3, in whom MP-RAGE after implantation was converted directly to the MNI standard space due to the technical issue related to the brain after tumor resection. In patient 9 with SEEG, the anatomical locations of the electrode leads were checked by the digital fusion of a post-implantation thin-sliced CT 3D image and coregistered to the MP-RAGE taken before implantation using CURRY 7 Neuroscan software (Compumedics, USA), which incorporates brain shift correction. Electrodes located in white matter were excluded in the present study. The electrodes' locations across the whole patients in the MNI space are shown in Fig. 1 (and Supplementary Figure 1).

The electrodes covered both the medial and lateral sides around the central sulcus. The anatomical parcellation of the stimulus sites was carried out in reference to the location of the midpoint of the pair of stimulating electrodes in the individual MRIs taken after grid implantation, similar to the previous study (Matsumoto et al., 2012, 2007), according to the parcellation scheme of the lateral and medial cortices, as mentioned below.
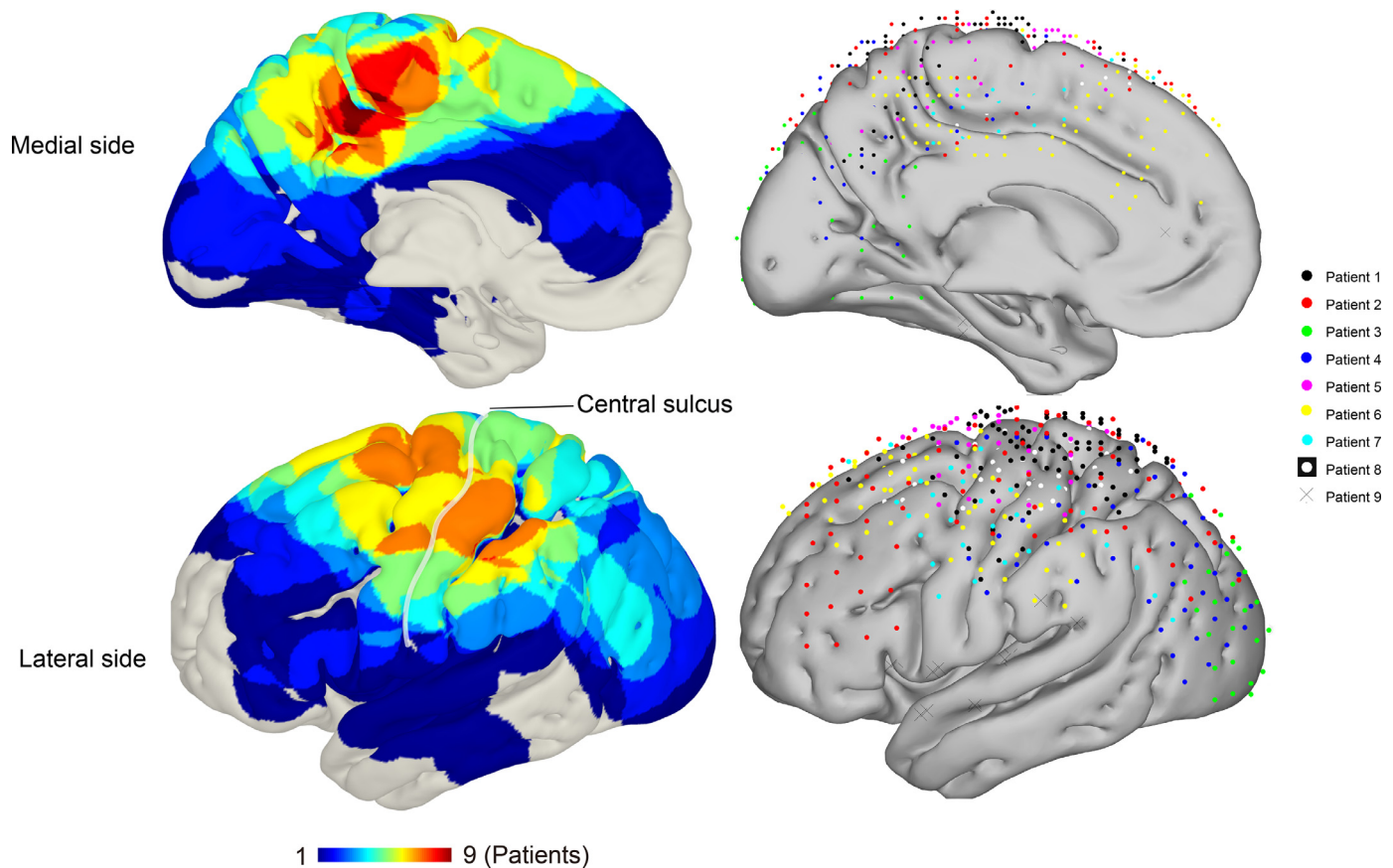
Fig. 1. Electrode coverage across all patients.

The stimulus sites and recording sites in all patients are plotted in Montreal Neurological Institute (MNI) standard space in the left side. Electrode density map was created by labeling each electrode coordinate in MNI space as 0 or 1 according to the location of each electrode across patients and by smoothing it with a gaussian filter (FWHM 15 mm) to obtain a 3D volume image. The color in the rainbow scale denotes the number of patients who had electrodes in the painted area. The cortical surfaces not painted in any color (i.e., gray) indicate that the cortical regions were not covered in any patient. On the right side, precise electrode locations were plotted by different colors according to the patient number.

2.3. Parcellation of the medial and lateral cortices

The boundaries and subdivisions of the medial parietal cortices were operationally defined according to recent proposals (Bzdok et al., 2015; Cavanna and Trimble, 2006; Hutchison et al., 2015; Margulies et al., 2009; Toga, 2015; Zhang et al., 2014).

The precuneus is limited anteriorly by the marginal branch of the cingulate sulcus, posteriorly by the medial portion of the parieto-occipital fissure, and inferiorly by the subparietal sulcus (Cavanna and Trimble, 2006). In the present study, the precuneus was subdivided into three parts by the precuneal sulcus: anterior, central, and posterior precuneus, according to the previously reported posterior-to-anterior functional subdivisions (Hutchison et al., 2015; Margulies et al., 2009; Zhang et al., 2014). The cingulate cortex is essentially divided into four parts: the perigenual anterior cingulate cortex (ACC), middle cingulate cortex (MCC), dorsal posterior cingulate cortex (dPCC), and ventral posterior cingulate cortex (vPCC) (Emmanuel et al., 2016; Vogt, 2009; Vogt et al., 1995, 2006). Accordingly, the ACC was defined as the region that surrounds the genu of the corpus callosum. The MCC was limited by the ACC anteriorly and by the ventral bank of the cingulate sulcus dorsally and terminated before the inflection of the marginal ramus of the cingulate sulcus (Emmanuel et al., 2016; Vogt, 2016). The posterior cingulate cortex (PCC) was defined as the region dorsal to the medial portion of the parieto-occipital fissure. The PCC was divided into the ventral part (vPCC) and dorsal part (dPCC) by the ventral branch of the splenial sulci. The PCL, supplementary motor area (SMA), and pre-supplementary motor area (pre-SMA) were included for the analysis in the medial frontal area. We illustrated the anatomical parcellations in which electrodes were implanted in the present study (Fig. 2).

In the lateral frontal cortex, we defined the dorsal half of the most caudal part of the middle frontal gyrus as the dorsal premotor area (PMd) in accordance with our previous CCEP studies (Matsumoto et al., 2012, 2007). The SPL, inferior parietal lobule (IPL), precentral gyrus (PrCG), and postcentral gyrus (PoCG) in the lateral frontal and parietal areas were also included in the analysis.

The whole anatomical parcellation in which electrodes were implanted in the present study was illustrated. The precuneus is limited inferiorly by the subparietal sulcus and subdivided into three parts by the precuneal sulcus, yielding the anterior, central, and posterior precuneus. See the methods section for details of the definition of parcellations.

2.4. CCEP recording and analysis

Details of the CCEP methodology have been described elsewhere (Kobayashi et al., 2017; Matsumoto et al., 2017, 2012, 2007; Matsumoto et al., 2004). Electrical stimuli consisted of a constant current square wave pulse lasting 0.3 ms, and the pulse frequency was 1 Hz with alternating polarity. The current intensity increased by 2 mA in a stepwise increment, to a maximum of 10 mA or until after-discharges were pro-
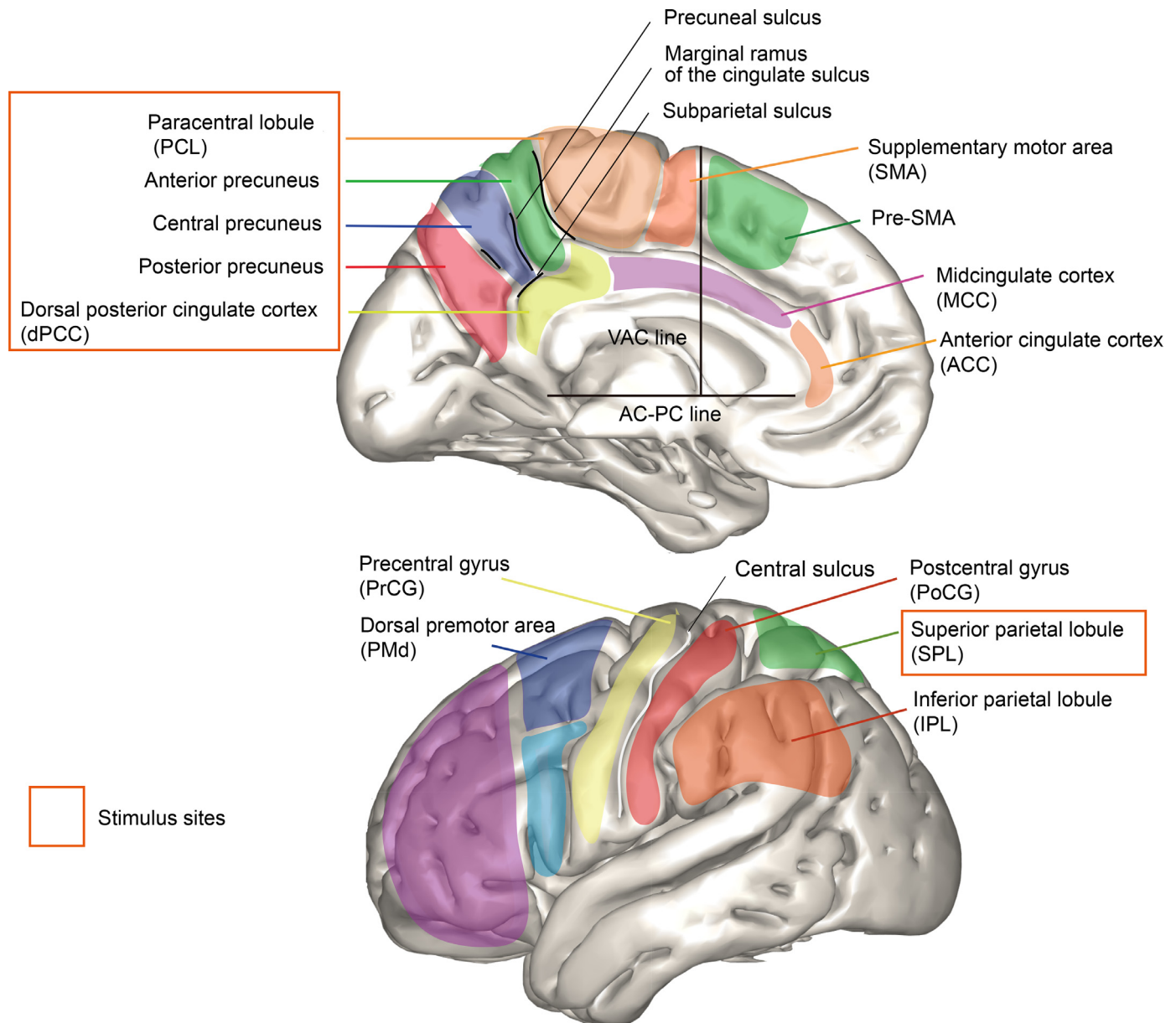
Fig. 2. Anatomical parcellation in the present study.

voked. ECoGs were recorded with a 0.08–300 Hz filter at a sampling rate of 1000 Hz (EEG-1100, Nihon Kohden, Tokyo, Japan) (in patients 1–8) or with a 0.08–600 Hz filter at a sampling rate of 2000 Hz (in patient 9). To obtain the CCEPs, we averaged ECoGs in a time-locked fashion to the stimuli by using in-house Matlab scripts applicable for off-line analysis (Matlab version 9.3.0; the MathWorks Inc., MA).

The electrical stimuli were delivered to the medial parietal cortices (a total of 38 pairs of electrodes) and SPL (a total of 21 pairs of electrodes). One electrode pair of electrodes was excluded because it was within a seizure onset zone (in the medial parietal cortices of patient 4). A total of ten pairs of electrodes in the medial parietal cortices and 14 pairs of electrodes in the SPL had interictal spikes during the presurgical evaluation. To standardize the CCEP N1 and N2 amplitude measurement, we defined the N1 and N2 amplitude as the height of a vertical line from the negative peak of N1 and N2, respectively to the intersection of the line between the onset to the offset of the N1 and N2 potential for each data point. The onset of N2 defined as the preceding positive trough (Matsumoto et al., 2004). We calculated the standard deviation (SD) of the amplitude during the baseline period (−100 ms to −5 ms

before stimulation). Based on the standard deviation, we calculated the z-score of the peak amplitude of N1 (and N2) by dividing the peak amplitude of N1 and N2 by the SD of the whole recording electrodes for each stimulation and determined the z-score as the strength of the response in each region. CCEPs were considered significant if the z-score of the N1 or N2 peak of the evoked potential exceeded the baseline amplitude by a threshold of $\pm$ 3 SD. Remote CCEP responses were defined as responses that were temporally discrete and at a distance of 25 mm or more from the stimulus electrodes. They were obtained from the frontal areas (a total of 8–72 electrodes were placed in the frontal area per patient), parietal areas (a total of 13–72 electrodes per patient), and occipital area (with a total of 30–39 electrodes per patient). Among the remote CCEP responses, we focused on the outstanding responses in terms of CCEP amplitudes. The predominant response was defined as the response showing the largest CCEP N1 with a latency of less than 50 ms, representing the main connection in each stimulation (one predominant response per stimulation). The additional response was defined as the response representing the other connections and showing the maximum N1 amplitude locally, without being a maximum amplitude as a whole

Table 1
Patient demographics.

Patient	1	2	3	4	5	6	7	8	9
Age, sex, handedness	27 F L	39 M R	40 M R	28 F R	44 M R	29 M L	24 M R	45 M R	25 F L
Epilepsy	OLE	FLE	FLE	PLE	FLE	FLE	OLE	FLE	TLE
Implanted hemisphere	R	L	L	R	R	R	R	L	R*
Ictal onset	Occipital lobe	Pre-SMA	Perirolandic area	Medial parietal (Precuneus)	SMA	Precentral gyrus	Occipital lobe	PMd	Medial temporal lobe
Pathology	FCDIIB	FCDIIB	Mixed oligo-astrocytoma	Low grade glioma	Mixed oligo-astrocytoma	FCDIIA	FCDIIA	FCDIIA	FCDIIA
electrode pairs stimulated	1 (dPCC) 1 (PCL) 4 (PrC) 6 (SPL)	5 (dPCC) 3 (PCL)	1 (PrC)	2 (PCL) 1 (PrC)	2 (PrC) 1 (SPL)	2 (dPCC) 1 (PCL) 1 (PrC) 4 (SPL)	2 (dPCC) 3 (PrC)	6 (PrC) 10 (SPL)	1 (PrC)
recording electrodes	72	108	56	48	48	100	52	100	84

* sEEG recording,DNET: dysembryoplastic neuroepithelial tumor, dPCC: dorsal posterior cingulate cortex, FCD: focal cortical dysplasia, FLE: frontal lobe epilepsy, OLE: occipital lobe epilepsy, PCL: paracentral lobule, PLE: parietal lobe epilepsy, PMd: dorsal premotor area, PrC: precuneus, preSMA: presupplementary motor area, sEEG: stereotactic electroencephalogram, SPL: superior parietal lobule.

(0–6 additional responses per stimulation). We defined upper limit of the N1 latency as 50 ms because the previous cluster analysis on more than 1500 CCEP responses commonly revealed an early N1 cluster with its peak less than 50 ms (Nakae et al., 2020 and Veit et al., 2021). This N1 peak definition is consistent with a previous SEEG study which showed the difference in CCEP between cortical stimulation and the white matter stimulation (Paulk et al., 2022).

To visualize the standardized connectivity map, we colored the MNI standard brain surface by the z-score of maximum amplitude of N1 and N2 after converting the electrode coordinates from the individual space to MNI standard space (Nakae et al., 2020). In painting the brain surface, the z-score at each electrode was smoothed with a Gaussian kernel (full width at half maximum [FWHM] 10 mm). The z-score was set to zero if no significant response was observed. The difference of electrode coverage in each patient was corrected by dividing the z-score map by the observation density map. The observation density map was obtained by smoothing the number of observations at each electrode with FWHM of 10 mm. It is the same as the electrode density map if we examine CCEP via just one stimulation site in the patient. We constructed the standardized connectivity map for the following two groups: 1) N1 responses with a peak latency of less than 50 ms, and 2) N2/late N1 responses with a peak latency of more than 50 ms. If the stimulus sites were in the right hemisphere, CCEP responses were flipped into the left hemisphere and we portrayed the left standard brain surface by the z-score (Nakae et al., 2020). We also illustrated connectivity maps in other conditions for confirming the effects of other confounding factors: with FWHM of 15 mm, excluding the patient 9 with SEEG, excluding the seizure onset zone in response sites, without thresholds of 3 SD of baseline amplitude for determining the significant responses.

2.5. Statistical analysis

We applied the permutation test to evaluate whether the differences in connectivity patterns among the medial parietal cortices were significantly above the chance level or not. The most important purpose of this study was to elucidate the differences in connectivity within the medial parietal cortices.

Therefore, we focused on the precuneus and dPCC in the statistical analysis. First, we listed the whole 29 stimulus sites in the two groups of the media parietal cortices (the precuneus, dPCC), and incorporated the z-score of the N1 responses into the list of the nine response regions (PMd, PrCG, PoCG, MCC, the precuneus, PCL, IPL, SPL, and the occipital cortex) by each stimulus site. We excluded the ACC and pre-SMA from the list of response regions since the electrodes did not cover these areas for the precuneus and dPCC stimulation. We also excluded electrodes with CCEP responses within 25 mm from the precuneus or dPCC stimulus sites since we focused on the remote responses in the present study. Therefore, we also had to exclude the dPCC as a response region since the length of dPCC was under 25 mm when we stimulated the dPCC. The sum of the z-score divided by the density of electrodes was calculated for each group of stimulus site and each response region. Due to the small number of stimulation sites in the anterior precuneus and posterior precuneus, we concatenated the three groups of stimulus sites (anterior, central, and posterior precuneus) into one group (precuneus) and performed the statistical analysis. As a result, 2×9 tables were constructed. Next, $\overline{Prc}$ and $\overline{dPCC}$ were used to denote the vector composed of nine z-scores in response regions when we stimulated the precuneus or dPCC, respectively. To evaluate the differences in the two vectors, the angle θ was computed using the inner products, as follows, and defined as the difference in the original data.

$$\theta_{org} = \cos^{-1}\left(\overline{Prc} \cdot \overline{dPCC}\right) / (|\overline{Prc}| \cdot |\overline{dPCC}|)$$

For the permutation test, the stimulus site labels (the precuneus, dPCC) were randomized and $\overline{Prc_{perm}}$ and $\overline{dPCC_{perm}}$ were computed. The

angle θ_{perm} was calculated by each randomized trial.

$$\theta_{perm} = \cos^{-1}\left(\overline{Prc_{perm}} \cdot \overline{dPCC_{perm}}\right) / \left(\left|\overline{Prc_{perm}}\right| \cdot \left|\overline{dPCC_{perm}}\right|\right)$$

A null distribution of θ_{perm} was generated by repeating this procedure 10,000 times. We considered a statistical significance if θ_{org} was out of the 95% confidence interval ($p < 0.05$) of the distribution of θ_{perm}.

We also performed the same permutation test after excluding patient 9 with SEEG.

2.6. Comparison with resting-state functional MRI connectivity

We intended to compare CCEP connectivity with functional connectivity derived from resting-state fMRI (rs-fMRI) data (Nakae et al., 2020). Firstly, we obtained the resting-state functional connectivity map from the rs-fMRI connectivity database (available on NeuroSynth website; http://neurosynth.org/) (Yarkoni et al., 2011). For each stimulus site of the medial parietal cortices, we obtained a functional connectivity map (3D volume image) by specifying coordinates that corresponded to the midpoint of each pair of stimulus electrodes as the seed voxel. We considered the voxels to be significant if the functional connectivity correlation value (Glanz Iljina et al., 2018) between the voxels and each stimulus site exceeded 0.15. The value of 0.15 was determined based on the previous study those methodologies were mainly used in Neurosynth (Yeo et al., 2011). The correlation values of significant voxels were obtained at each stimulus site, including the precuneus (anterior, central, and posterior), dPCC, PCL and SPL. If the stimulus sites were in the right hemisphere, the functionally correlated area was flipped into the left hemisphere, and we portrayed the left standard brain surface by the averaged correlated value. We showed the areas whose correlation value was more than 0.15 overlapping the areas showing significant CCEP responses in 3D standardized map in Supplementary Figure 8.

3. Results

3.1. CCEP responses

The electrode locations and CCEP waveforms in a representative patient (patient 1) were shown for the stimulation of the PCL, anterior precuneus, and central precuneus (Fig. 3). When the stimulus site was shifted to the adjacent pair of electrodes, the CCEP distribution was obviously changed. CCEP responses in each patient were illustrated in Supplementary Figure 9 A–H.

Tables 2A and 2B show the results of predominant and additional N1 responses across patients.

In terms of the spatial distribution of CCEP responses, the anterior precuneus stimulation elicited the N1 responses in the PMd, precentral gyrus, postcentral gyrus, and precuneus (only the most four active regions were shown hereafter). Stimulation of the central precuneus showed N1 responses in the IPL, SPL, occipital cortex, and PMd. Stimulation of the posterior precuneus showed responses in the occipital cortex, IPL, SPL, and PCL. Overall, the precuneus stimulation (19 sites across all patients) elicited the predominant/additional N1 in the IPL (4 predominant/4 additional responses), the occipital cortex (1/8 responses), SPL (1/5 responses), and PMd (1/2 responses), as the most active 4 regions. No predominant/additional N1 was elicited in the middle cingulate cortex, suggesting that the precuneus mainly connects to the lateral parieto-frontal and occipital areas.

Stimulation of dPCC elicited N1 responses in the middle cingulate cortices, SPL, the precuneus, and IPL (the most active 4 regions), while no predominant/additional N1 was recorded in PMd. Based on these results, in contrast to the precuneus, dPCC tended to connect to the medial frontal cortex rather than the lateral frontal cortex. The difference in mean z-scores in response regions between the precuneus stimuli and dPCC stimuli were shown in Fig. 4. The largest amplitude was noted in IPL for the precuneus stimulation, and in MCC for the dPCC stimulation.

Table 2
Summary of the CCEP recordings for each stimulus site.

Stimulus	Number of outbound connections (Predominant – additional connections)												
Anatomical Parcellation	Number of stimulus sites (pairs)	PMd	Pre-central gyrus	Post-central gyrus	MCC	dPCC	Precuneus	PCL	IPL	SPL	Occipital cortex	ACC	Pre-SMA
Anterior precuneus	5	1–1	1–0	1–0	0–0	0–0	1–0	0–0	0–1	0–1	0–1	n.a.	n.a.
Central precuneus	10	0–3	0–0	0–1	0–0	0–0	0–0	0–2	4–2	4–3	0–4 (SOZ:2)	n.a.	n.a.
Posterior precuneus	4	0–0	0–0	0–0	0–0	0–0	0–0	0–1	1–1	1–0	1–3 (SOZ:1)	n.a.	n.a.
dPCC	10	0–0	0–1	0–1	5–0 (SOZ:2)	n.a.	1–1	0–0	0–3	3–1	0–2	n.a.	n.a.
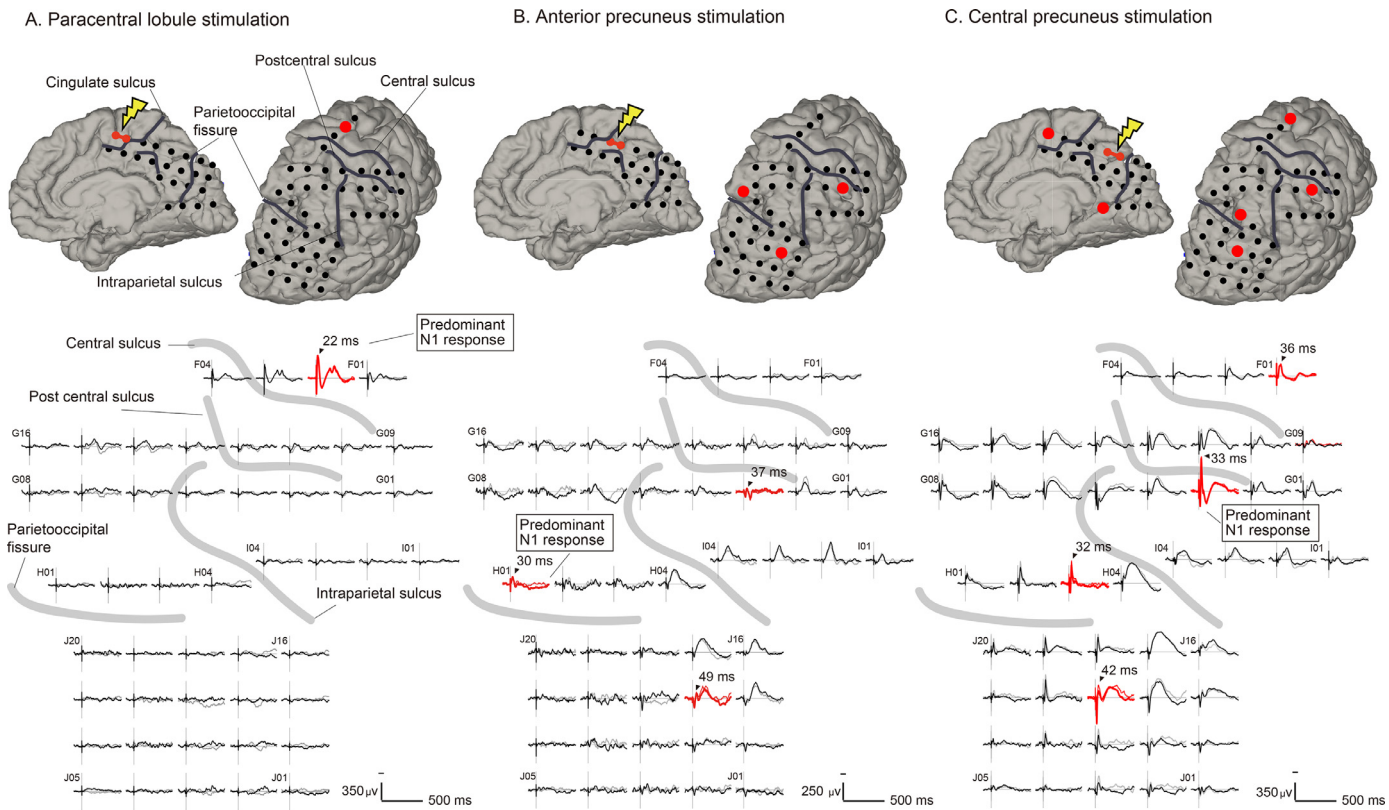
Fig. 3. CCEP findings in a representative patient (patient 1). .

Fig. 4. Mean N1 amplitude (z-score) in each parcellation for the precuneus and dPCC stimulation.
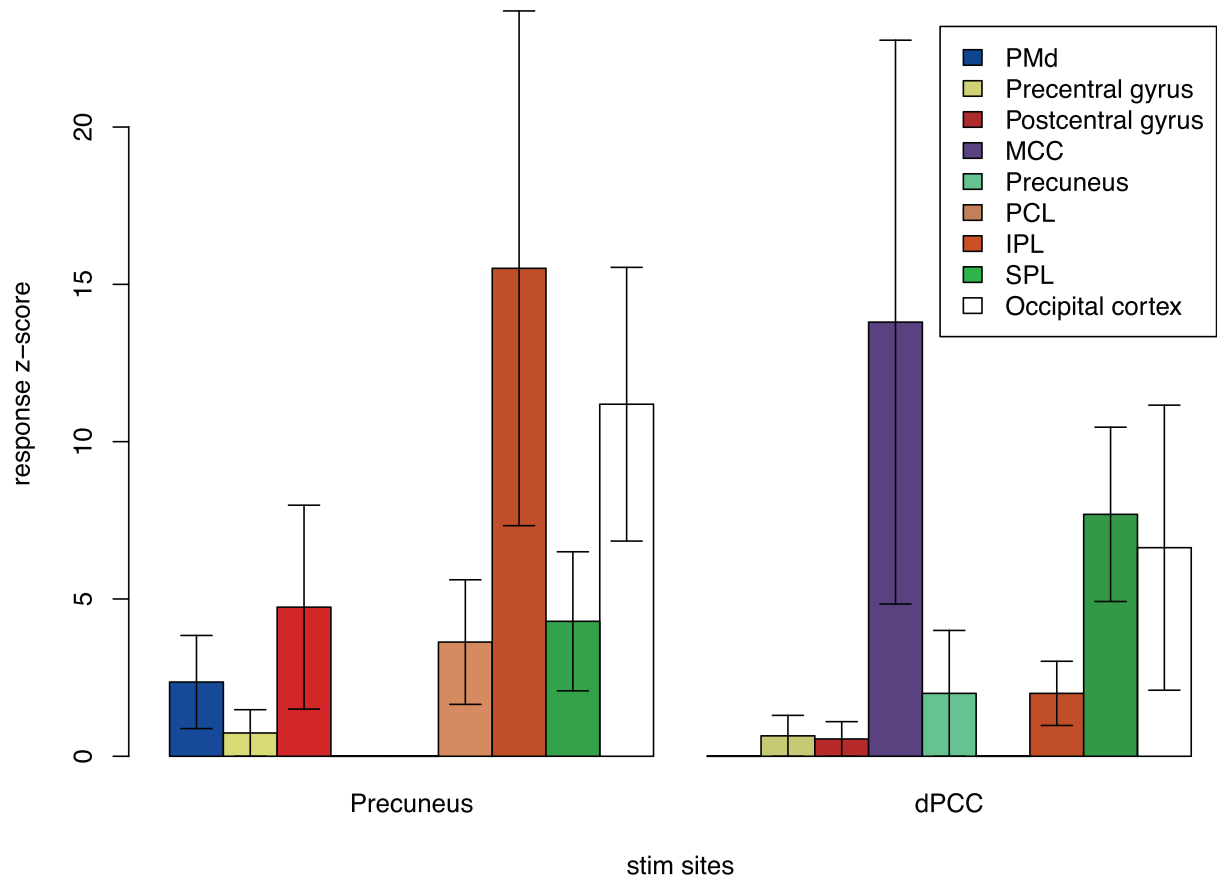
Table 2B

.

Stimulus		Number of outbound connections (Predominant – additional connections)												
Anatomical Parcellation	Number of stimulus sites (pairs)	PMd	Pre-central gyrus	Post-central gyrus	MCC	dPCC	Precuneus	PCL	IPL	SPL	Occipital cortex	ACC	Pre-SMA
PCL	9	1-2	4-3	3-0	0-0	0-0	0-0	0-0	0-2	0-0	0-0	1-0 (SOZ:1)	0-1 (SOZ:1)
SPL	21	1-1	5-2	0-1	0-1	0-0	4-2	1-2	0-3	3-1	0-3 (SOZ:1)	n.a.	n.a.

ACC: anterior cingulate cortex, dPCC: dorsal posterior cingulate cortex, IPL: inferior parietal lobule, MCC: midcingulate cortex, PCL: paracentral lobule, PMd: dorsal premotor area, PrC: precuneus, pre-SMA: presupplementary motor area, SPL: superior parietal lobule, SOZ: seizure onset zone.
n.a.: not available due to the lack of electrode coverage.

There was no significant difference in the amplitude in each area between the precuneus and dPCC stimuli (multiple comparison with Bonferroni's method).

Stimulation of PCL yielded CCEPs in the precentral gyrus, postcentral gyrus, PMd, and IPL. Thus, the PCL was mainly connected with the area around the precentral gyrus. SPL stimulation yielded responses in the precentral gyrus, the precuneus, SPL, and PCL. Conversely, the stimulation of either the precuneus or dPCC elicited predominant/additional CCEPs in the SPL. These findings suggest a possible bidirectional connection between the SPL and the medial parietal cortices. As for the involvement of response sites in the seizure onset zone or irritative zone, out of 92 response sites, one electrode in the anterior cingulate cortex, one in the pre-SMA, two in the midcingulate cortex, and four in the occipital cortex was involved in the seizure onset zone. A total of two electrodes in the postcentral gyrus, four in the occipital lobe, four in SPL, seven in the medial parietal cortices, and seven in IPL had interictal spikes during the presurgical evaluation.

On 3D MRI, the stimulus sites are shown as a pair of interconnected red electrodes, and black electrodes represent recording electrodes. CCEPs on the lateral convexity are plotted in reference to the major sulci identified on 3D MRI (A–C). PCL stimulation elicited a predominant N1 response (N1≤50 ms) in the precentral gyrus without any additional responses (A). Stimulation of the anterior precuneus showed a predominant response in SPL and additional responses in the IPL (the supramarginal gyrus) and occipital area (B). Stimulation of the central precuneus revealed a predominant response in the IPL (the supramarginal gyrus) and additional responses in the SPL, PMd and the occipital area (C). CCEPs with N1 latencies over 50 ms or the amplitude less than 3 SD of the baseline activity (from −100 ms to −5 ms) were excluded for the CCEP N1 connectivity analysis.

The mean N1 amplitude (z-score) was shown for each response region for the two stimulus sites, the precuneus (combining the three subdivisions—anterior, central, and posterior precuneus) and dPCC. Some differences were noted in the connectivity pattern. The precuneus stimulation elicited responses in PMd or PCL, while dPCC stimulation did not. In contrast, dPCC stimulation elicited responses in MCC, while the precuneus stimulation did not. The largest amplitude was noted in IPL for the precuneus stimulation, and in MCC for the dPCC stimulation. The error bars represented the standardized error. dPCC: dorsal posterior cingulate cortex, IPL: inferior parietal lobule, MCC: midcingulate cortex, PCL: paracentral lobule, PMd: dorsal premotor area, SPL: superior parietal lobule

3.2. 3D visualization of CCEP responses in the MNI standardized space

The frontal and parietal area showing N1 CCEP responses with latencies under 50 ms across patients (patients 1–9) are displayed together in the MNI standard space (Fig. 5). Two types of maps (cut-off z-value = 3 or 10) were illustrated.

The different spatial connectivity patterns within the medial parietal cortices were also confirmed in this 3D view. The central and posterior precuneus stimuli elicited responses in the lateral parietal area, including the supramarginal gyrus and angular gyrus, as well as the anterior part of the lateral occipital cortex. We did not mention these areas for 3D visualization because the medial occipital cortex and posterior part of the lateral occipital cortex was covered in less than three patients (Fig. 1). Meanwhile, dPCC stimuli elicited responses in the medial frontal area and IPL. Within the precuneus, the anterior precuneus tended to connect with the lateral frontal area, especially the PMd, while the central and posterior precuneus connected with the lateral frontal area.

We also showed the areas presenting N2/late N1 responses with latencies over 50 ms (Fig. 6, with two cut-off z values), standardized maps with FWHM of 15 mm (Supplementary Figure 4), excluding the patient 9 with SEEG (Supplementary Figure 5), excluding the seizure onset zone in response sites (Supplementary Figure 6), without thresholds of 3 SD
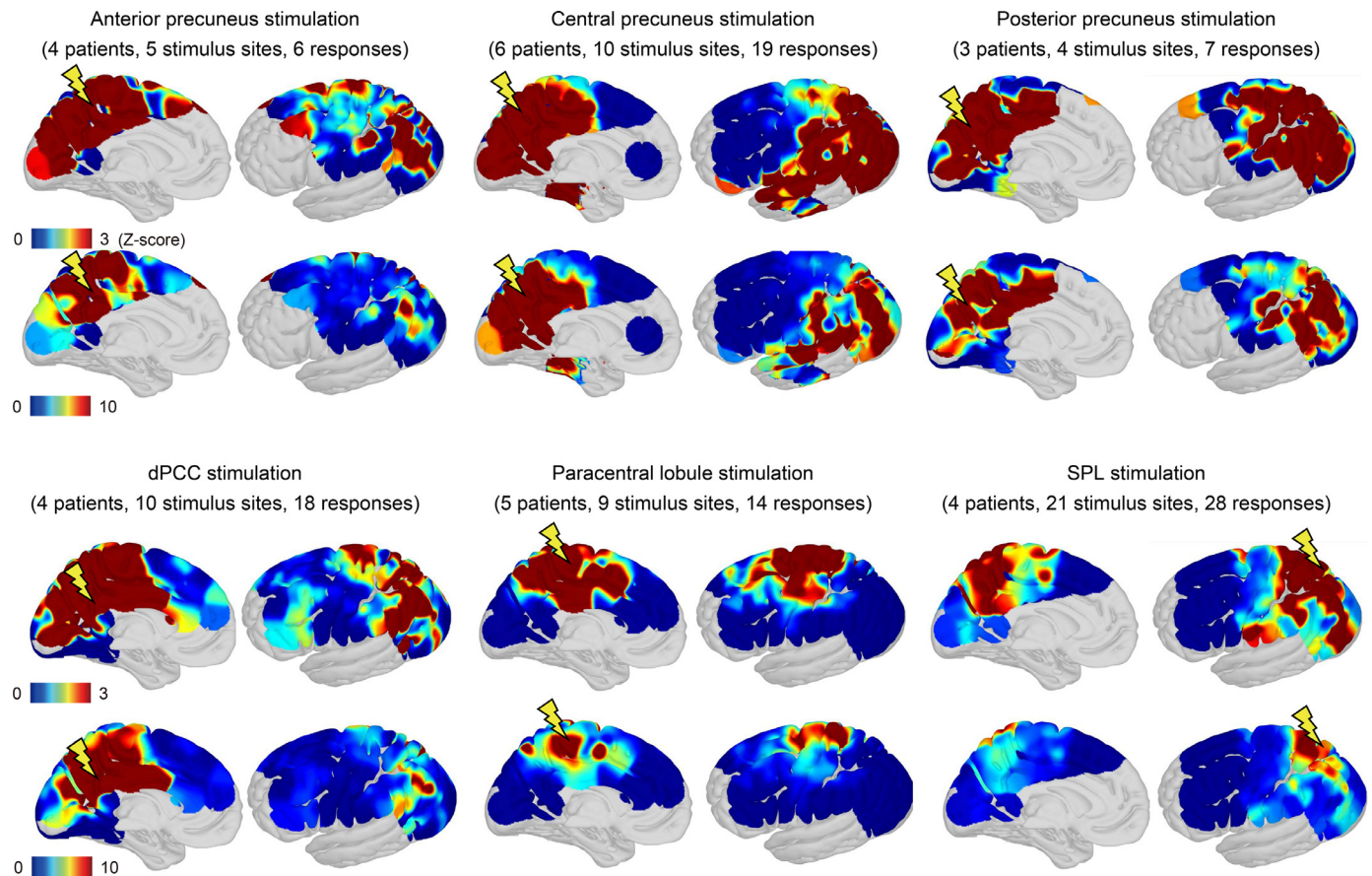
Fig. 5. 3D Visualization of N1 CCEP responses (activities with a peak latency of N1 ≤ 50 ms).

of baseline amplitude for determining the significant responses (Supplementary Figure 7). These standardized maps with various conditions revealed similar spatial distribution to those of the original standardized map such as MCC involvement in dPCC stimulation.

Although the distribution pattern of responses was similar to that of N1 response regions seen in Fig. 5, several differences existed between N1 responses and N2/late N1 responses. The central precuneus, posterior precuneus, dPCC, and PCL showed additional connectivity with the lateral prefrontal and premotor areas in N2/late N1 responses.

Regarding the spatial distribution of CCEP N1 responses, the hypothesis that the precuneus and dPCC stimulation elicits different connectivity patterns were evaluated by performing the permutation test with randomized 2 stimulus sites (the precuneus, dPCC) and 9 response regions (PMd, the precentral gyrus, the postcentral gyrus, MCC, the precuneus, PCL, IPL, SPL, and the occipital lobe). The test revealed a significant difference between randomized trials and the original data (*P*<0.05, Supplementary Figure 2), supporting the hypothesis that the precuneus and dPCC had different connectivity patterns. However, when we exclude patient 9 with SEEG, the difference was not significant between the dPCC and the precuneus stimuli.

The spatial distribution of CCEP responses, in particular N2/late N1 responses, was partly similar to that of resting-state functional connectivity (rs-FC) obtained from the NeuroSynth database using the anterior precuneus, PCL, or SPL stimulus site as a seed ROI (Supplementary Figure 3). The anterior precuneus ROI was functionally connected with the prefrontal area, the supramarginal gyrus, and the lateral occipital area. The PCL ROI was functionally connected with the precentral and postcentral gyri. The SPL ROI was functionally connected with the IPL and lateral occipital area. While these aforementioned areas had similar connectivity patterns between the two different measures, we found a

difference in the lateral occipital area, which showed connectivity with the central and posterior precuneus in CCEP connectivity in the maps with cut-off z-values of 3, but less connectivity in terms of rs-fMRI connectivity. Both N1 and N2 responses in the lateral occipital areas were weaker in the maps with a cut-off z-value of 10 compared to those with a cut-off z-value of 3. Overlapping areas both functional connectivity and CCEP responses were shown in Supplementary Figure 8A (N1 response) and Supplementary Figure 8B (lateN1/N2 response).

With regard to the N1 responses, a clear difference was observed in the connectivity patterns between the dorsolateral frontal area and the three medial parietal regions (the central precuneus, posterior precuneus, dPCC). Indeed, connectivity between the dorsolateral frontal area and the medial parietal regions existed in rs-fMRI but did not exist in CCEP analysis.

The average N1 response map was shown in the Montreal Neurological Institute (MNI) standard space. The color painted on the brain denotes the amplitude of average N1 responses. See the main text for the details regarding the generation of the MNI average map. The area painted in white showed that no electrode was placed. Two types of maps (cut-off z-value = 3 or 10) were illustrated.

Note that the average response map originally featured a z-value for the amplitude but was smoothed by a Gaussian kernel (FWHM 10 mm) for visualization. The Gaussian smoothing blurs the values across the adjacent voxels while keeping the sum, such that the values decrease after smoothing. The accurate localization of the N1 responses in the individual brain were shown in Table 2. dPCC: dorsal posterior cingulate cortex, SPL: superior parietal lobule

The average N2 response map was shown in the Montreal Neurological Institute (MNI) standard space. N2 response (or late N1 response) with latencies over 50 ms are shown. Two types of maps (cut-off z-
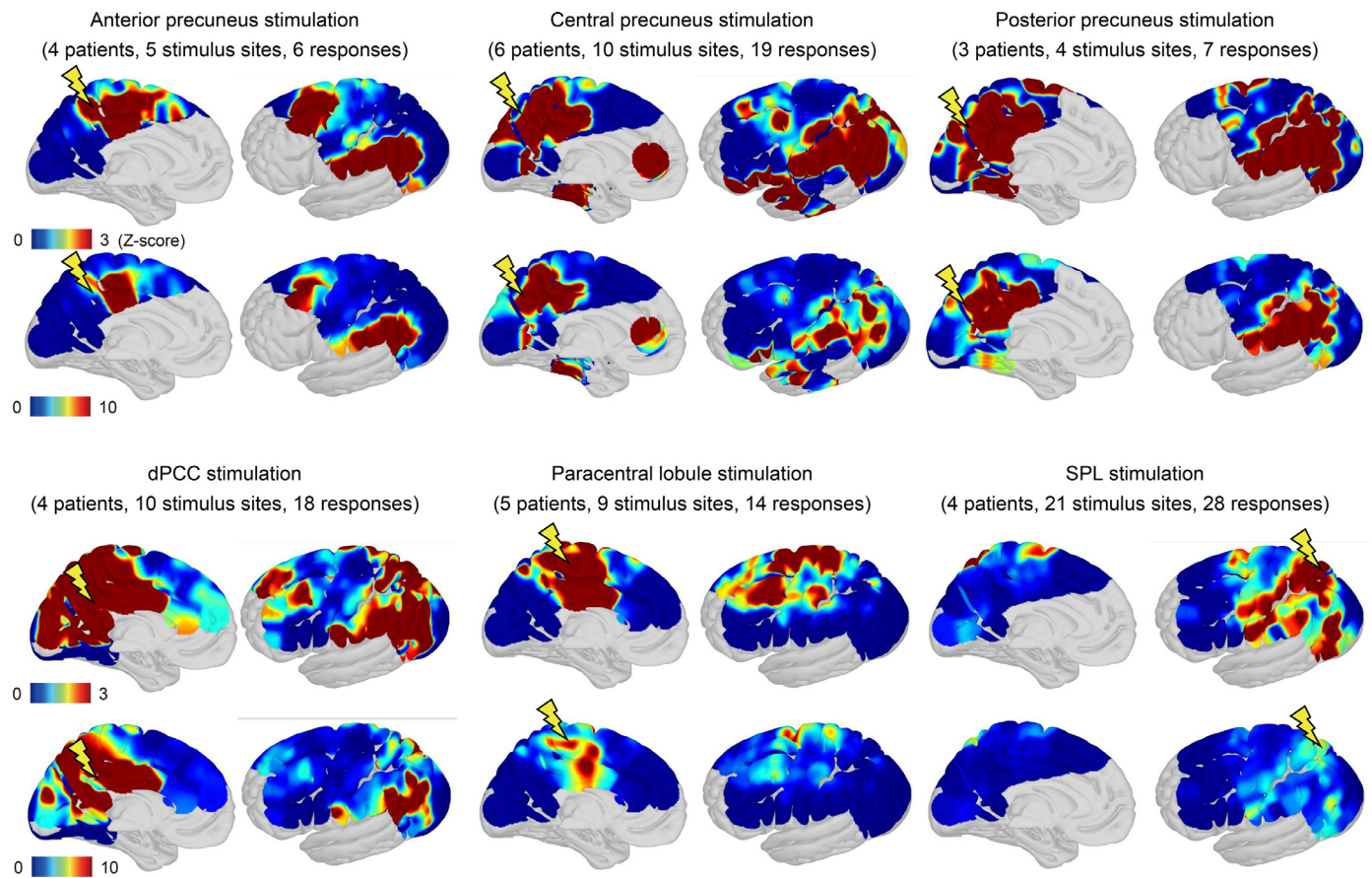
Fig. 6. 3D Visualization of N2/late N1 CCEP responses (activities with peak latency ≥ 50 ms).

value = 3 or 10) were illustrated. Note that the spatial distribution was wider than that of N1 responses. dPCC: dorsal posterior cingulate cortex, SPL: superior parietal lobule

4. Discussion

By means of an effective connectivity analysis using single-pulse electrical cortical stimulation, we assessed the connectivity patterns from each medial parietal parcellation and constructed a standardized CCEP connectivity map in the MNI space. It was characterized by the distinctive connectivity pattern within the medial parietal cortices. The precuneus connected to the IPL, SPL, the anterior part of lateral occipital areas, and the dorsal premotor area. Meanwhile, the dPCC connected with the medial frontal lobe, SPL, and IPL.

The spatial connectivity patterns between these areas were significantly different. Several parameters for visualization (the value of FWHM) or clinical factors (including SEEG case or recording electrodes in seizure onset zone) could affect the results. Therefore, we performed analysis excluding these factors and achieved similar results as described above. The modes of connectivity can be discussed in the context of the functional organization of the medial parieto-frontal circuit associated with visual-motor integration and the DMN.

4.1. Effective connectivity of the medial parietal cortices by CCEPs

In terms of the two-dimensional exploration of connectivity patterns on the cortical surface, the subdural grid allows us to stimulate the cortical surface and record CCEP responses more densely at spatial resolution reflective of the inter-electrode distance (1 cm), compared to the SEEG, in which depth electrodes are inserted sparsely (∼3 cm apart each). Most of the previous human CCEP studies on the medial pari-

etal cortices used depth electrodes (SEEG), except for one study which employed subdural electrodes (Entz et al., 2014). Other previous studies using SEEG have shown that PCC stimulation elicited bilateral medial temporo-parieto-occipital responses, including in the hippocampus and lateral parieto-occipital areas including IPL and SPL (Enatsu et al., 2014, 2015; Kubota et al., 2013). Donos et al., have demonstrated the outbound connections from the precuneus, dPCC, PCL and SPL. They revealed the connection between the PCL and the precentral gyrus or the postcentral gyrus. They also demonstrated the connection between the precuneus and premotor area or occipital cortex, which is consistent with our findings (Donos et al., 2016). Non-human primate studies revealed that the PCC sends connections to the dorsal prefrontal cortex and parieto-temporal cortex (posterior part of IPL) (Pandya et al., 1981). According to the human functional connectivity patterns using resting-state fMRI, the dPCC connects with the middle cingulate cortex (Cha et al., 2017). The CCEP responses were recorded only in the frontal or parieto-occipital lobes in the present study since the temporal lobe was not covered by electrodes for clinical reasons. Although the distance between the dPCC and MCC is relatively small, the response of the MCC was not solely accounted for by this closeness. This was because the stimulation of the PCL, which was also close to the MCC, did not evoke CCEP responses in the MCC. In Figs. 5 and 6, although the precuneus stimulation seemed to elicit responses in the caudal part of the MCC, this was due to the Gaussian spatial filtering applied for plotting CCEP responses on the MNI space. The precise locations of the CCEP responses were determined according to personal brain MRI scans, as shown in Table 2.

The difference in connectivity between the anterior and central/posterior precuneus we observed can be linked to motor-related functions: the posterior precuneus - occipital cortex connection can subserve visual-associated functions, while the anterior precuneus-PMd

connection can subserve visually guided, externally directed movement. Connections between the precuneus and lateral parietal areas or premotor areas seem to play a pivotal role in motor-related functions such as visual-guided hand movement (Caminiti et al., 1999; Cavanna and Trimble, 2006; Bernier and Grafton, 2010; Fernandez-Ruiz et al., 2007). In contrast to the anterior precuneus, a macaque tracer or resting-state functional connectivity study showed that the PO area, a homolog of the human central/posterior precuneus, had a strong connection with prestriate areas within the parieto-occipital fissure and the cuneus subserving the processing of visuospatial information processing (Colby et al., 1988; Margulies et al., 2009). Taken together, these findings indicated that the anterior and central/posterior precuneus were associated, in particular, with visually guided motor-related functions.

Judging from the present CCEP findings, the dPCC is connected with the medial frontal area, SPL and IPL, whereas the precuneus was connected with IPL, the anterior part of the lateral occipital cortex, SPL, and the dorsal premotor area. Considering the functional differences between the precuneus and dPCC, namely the visual/motor-related functions of the precuneus, and the internally directed cognition or the resting state activation of the dPCC (Fox et al., 2018), the distinct connectivity pattern in the medial parietal cortices could support such functional differentiation.

Regarding the association between DMN and connectivity patterns in the present study, a part of the connectivity of the central and posterior precuneus resembled that of the dPCC. Meanwhile the connectivity from the anterior precuneus is different from that of dPCC. Although previous works on resting-state connectivity or diffusion tensor imaging showed that the ventral posterior medial cortex is the core of DMN (Utevsky et al., 2014; Zhang et al., 2014), dPCC connectivity in the present study did not completely overlap with the connectivity of DMN because dPCC connected with the SPL. One possible explanation for the disconcordance is the involvement of the frontoparietal cognitive network. Since the frontoparietal cognitive network included a part of the ventral medial parietal cortex (Yeo et al., 2011), dPCC stimulation could have involved the frontoparietal cognitive network in addition to DMN.

As for SPL connectivity, the present study successfully added further information to our previous CCEP study on the front-parietal network (Matsumoto et al., 2012). Electrophysiologically, the bidirectional connections were present between the SPL and regions such as the PMd, occipital area, and precuneus. Connections between the anterior part of the SPL and PMd have been documented in the macaque using tracers (Hoshi and Tanji, 2007; Johnson et al., 1996; Matelli et al., 1998). In humans, the anterior and mid-lateral part of the SPL also demonstrated functionally connectivity with the PMd (Wang et al., 2015). These connections are supposed to provide information related to the spatial representation of the body parts or visual information or attention (Wang et al., 2015; Mars et al., 2011; Humphreys and Lambon Ralph, 2015; Leichnetz, 2001; Caminiti et al., 1999).

The functional connectivity shown in Supplementary Figure 3 partly resembles the results of CCEP connectivity, in particular the N2/late N1 responses in Fig. 6. The relatively good consistency between the two methods has been addressed previously (Keller et al., 2014a; Nakae et al., 2020). The precise generation mechanism of N2 responses was not fully understood, although the responses were supposed to be related to polysynaptic responses or inhibitory rebounds (Paulk et al., 2022). A recent study suggested the different functions within N2 responses. Veit et al., revealed the responses with both N1 and N2 are more likely to be found when the stimulated and recorded sites belong to the same intrinsic networks, while isolated N2 reactions are more likely elicited when they belong to different intrinsic networks (Veit et al., 2021). In the present study, we did not distinguish the N2 responses from this viewpoint. The proposed difference between the two N2 types (i.e., with or without N1) may explain the overlapping of the functional connectivity and the CCEP responses, but these two kinds of connectivity patterns did not completely overlap with each other. The CCEP

connectivity provided connectivity information not obtained by a functional connectivity analysis, such as the connection between the central or posterior precuneus and the anterior part of the lateral occipital cortex. The inconsistency between the two methods may be partly attributed to the differences in methods between the CCEP and rs-fMRI, or the cut-off z-value. Standardized maps with a cut-off z-value of 10 revealed weaker responses in the anterior part of the lateral occipital cortex and stronger responses mainly in the parietal lobe.

4.2. Clinical implications

Since the medial parietal cortices are involved in various motor, visual, or cognitive functions as discussed above, seizures arising from the area revealed a wide range of semiologies. The present CCEP connectivity findings can help understand these semiologies and seizure network arising from the medial parietal cortices. Seizures arising from the posterior cingulate can cause motor symptoms such as hypermotor (hyperkinetic) seizures, asymmetric tonic-clonic seizures, automotor seizures, focal to bilateral tonic-clonic seizures, or auras (Déjà vu, jamais vu, abdominal) as ictal semiology patterns (Enatsu et al., 2014; Alkawadri et al., 2013). These three types of seizure semiology patterns are presumed to manifest as a result of the ictal spreading of epileptic activity from the posterior cingulate to the anterior/middle cingulate cortex, SMA and mesial temporal lobe. The present study revealed the connectivity pattern between the posterior cingulate cortex and medial frontal lobe, such as the middle cingulate cortex, explaining the semiology pattern of hypermotor (hyperkinetic) seizures. Although the dPCC did not directly connect with SMA directly, the middle cingulate cortex was reported to be connected with either the SMA or the anterior cingulate cortex. It is possible that the epileptic focus at dPCC could manifest these different seizure types by the ictal propagation through these indirect connections (Caruana et al., 2018).

Our results showed that the anterior precuneus tended to connect with the lateral frontal area, whereas the central and posterior precuneus had a rich connection with the occipital lobe. This is consistent with reports that described the ictal semiology arising from the epileptic focus in the precuneus (Al-Ramadhani et al., 2021). Seizures from the anterior precuneus showed the semiology of bilateral tonic posturing suggesting propagation to the SMA with ECoG findings (Umeoka et al., 2007), those from the posterior precuneus revealed visual distortion with macropsia and micropsia (Mailo and Tang-Wai, 2015). One case series also showed that two patients with lesions in the anterior half of the precuneus had body movement such as clonic jerks or increased muscle tone, whereas another two patients with lesions in the posterior half experienced visual symptoms such as twirling vision or visual distortion (Harroud et al., 2017). Mailo and Tang-Wai also reported the seizure semiology of urge described as a "feeling of wanting to move" and mentioned that the semiology was accompanied by the ictal pattern localized to the parieto-occipital region during video-EEG monitoring. Although there was unexplainable semiology such as disability of sound recognition or vestibular function (Saeki et al., 2009; Wiest et al., 2004), several types of seizure semiology patterns can be explained by the spread of epileptic activity from the focus to either the lateral frontal or occipital area through the connections revealed by the present CCEP study.

4.3. Limitations

Some limitations should be noted in the present study. First, the total number of patients was limited, and the location of the electrode grids was reflective of clinical goals. Not all patients had electrode coverage over the medial frontal, lateral frontal, or occipital cortex and the investigated region was constrained to the layout of the electrode grid in each patient. Moreover, the lack of simultaneous coverage is noted. Since the anatomical coverages of stimulus/recording electrodes in the medial parietal cortices were sparse and different in each patient, our

results provided differences in connections in the limited patch of the brain investigated in the present study.

We could not evaluate the connectivity difference between left and right hemisphere stimulation since the present study included only 3 patients with left implanted electrodes. However, except for the pre-SMA or ACC, all cortical parcellations assessed in the present study were covered in more than two patients. Therefore, we concluded that the connectivity pattern was not based on the results of a single patient.

Second, although the stimulus sites and the majority of response regions were away from the epileptic focus, the effect of pathology, namely the epileptic brain, cannot be excluded. We could not exclude the seizure onset zone in response sites because of the small numbers of the patients and response electrodes. However, seizure onset zones were far from the medial parietal cortices in 8 out of 9 patients. In the remaining patient, we excluded electrodes in the seizure onset zone from the analysis. Since subdural grids were implanted in the medial parietal areas only if the areas were involved in the seizure onset zone or epileptic networks, the possibility of the electrodes being involved in the seizure onset zone or showing interictal spikes is inevitable. Therefore, we could not exclude electrodes with interictal spikes from the stimulus and response electrodes; however, we carefully minimized the effects of network modifications due to epilepsy by excluding the seizure onset zone from stimulus site. Further cases are needed to validate the connectivity pattern revealed by the present study.

Third, we did not apply other methods such as Granger causality or transfer entropy to resting ECoG data for determining the directed causal influence. Future studies using these methods would complement the present CCEP connectivity findings for better understanding of the dPCC and precuneus connectivity in humans.

Fourth, we included one patient with SEEG implantation. Although detailed parameter analyses of CCEP using SEEG were performed recently (Paulk et al., 2022), the precise difference between CCEP of SDG cases and that of SEEG cases has not yet been clarified. CCEP patterns between SDG and SEEG might be different, and further accumulation of CCEP data with SDG implantation will delineate the connectivity patterns from/to the dPCC and precuneus.

Lastly, since we could not analyze the resting state data from these patients with the same sites, future work combining CCEP, and rest-fMRI data will shed light on the relationships between them and the electrophysiological basis of resting-state functional connectivity.

4.4. Conclusions

A standardized CCEP connectivity map revealed different connectivity patterns in the human medial parietal cortices. The precuneus was connected with IPL, the anterior part of lateral occipital area, SPL, the dorsal premotor area, whereas the dPCC was connected with the medial frontal area, SPL, and IPL. Moreover, CCEP connectivity patterns are partly consistent with those obtained from the functional connectivity database. A standardized CCEP connectivity map would be useful as a reference for non-invasive connectome studies. Future inter-institutional collaborations with a larger patient cohort will help lay the foundation of a standardized CCEP connectivity map for human connectome research.

Declaration of Competing Interest

The Departments of Epilepsy, Movement Disorders and Physiology are an endowment department, supported with a grant from Eizai Co., Ltd., NIHON KOHDEN CORPORATION, Otsuka Pharmaceutical Co., Ltd., and UCB Japan Co., Ltd.

Credit authorship contribution statement

Masaya Togo: Conceptualization, Methodology, Investigation, Writing – original draft, Writing – review & editing, Funding acquisition.

Riki Matsumoto: Conceptualization, Methodology, Writing – review & editing, Project administration, Funding acquisition. **Kiyohide Usami:** Methodology, Validation, Data curation, Writing – review & editing. **Katsuya Kobayashi:** Methodology, Validation, Data curation, Writing – review & editing. **Hirofumi Takeyama:** Methodology, Validation, Data curation. **Takuro Nakae:** Methodology, Software, Validation, Data curation. **Akihiro Shimotake:** Methodology, Validation, Data curation. **Takayuki Kikuchi:** Resources, Data curation. **Kazumichi Yoshida:** Resources, Data curation. **Masao Matsuhashi:** Methodology, Software, Validation, Data curation. **Takeharu Kunieda:** Resources, Data curation, Supervision. **Susumu Miyamoto:** Supervision. **Ryosuke Takahashi:** Supervision. **Akio Ikeda:** Conceptualization, Methodology, Writing – review & editing, Project administration, Funding acquisition.

Data Availability

Data will be made available on request.

Data availability

The data that support the findings of this study are not publicly available because of privacy or ethical restrictions. The de-identified data can be available from the corresponding author on reasonable request and completion of a formal data sharing agreement.

Code availability

All code used to generate the findings of this study are available upon request. The used software and functions are stated at appropriate location in the manuscript in the Methods section.

Acknowledgements

Supplementary materials

Supplementary material associated with this article can be found, in the online version, at doi:10.1016/j.neuroimage.2022.119639.

References

Alkawadri, R., So, N.K., Van Ness, P.C., Alexopoulos, A.V., 2013. Cingulate epilepsy: report of 3 electroclinical subtypes with surgical outcomes. JAMA Neurol. 70, 995–1002.
Al-Ramadhani, R.R., Shivamurthy, V.K.N., Elkins, K., Gedela, S., Pedersen, N.P., Kheder, A., 2021. The precuneal cortex: anatomy and seizure semiology. Epileptic Disord. 23, 218–227.
Andrews-Hanna, J.R., Smallwood, J., Spreng, R.N., 2014. The default network and self-generated thought: component processes, dynamic control, and clinical relevance. Ann. N. Y. Acad. Sci. 1316, 29–52.
Arbune, A.A., Popa, I., Mindruta, I., Beniczky, S., Donos, C., Daneasa, A., Mălîia, M.D., Băjenaru, O.A., Ciurea, J., Barborica, A., 2020. Sleep modulates effective connectivity: a study using intracranial stimulation and recording. Clin. Neurophysiol. 131, 529–541.
Bernier, P.M., Grafton, S.T., 2010. Human posterior parietal cortex flexibly determines reference frames for reaching based on sensory context. Neuron 68, 776–788.
Bzdok, D., Heeger, A., Langner, R., Laird, A.R., Fox, P.T., Palomero-Gallagher, N., Vogt, B.A., Zilles, K., Eickhoff, S.B., 2015. Subspecialization in the human posterior medial cortex. Neuroimage 106, 55–71.
Caminiti, R., Genovesio, A., Marconi, B., Mayer, A.B., Onorati, P., Ferraina, S., Mitsuda, T., Giannetti, S., Squatrito, S., Maioli, M.G., 1999. Early coding of reaching: frontal and parietal association connections of parieto-occipital cortex. Eur. J. Neurosci. 11, 3339–3345.
Caruana, F., Gerbella, M., Avanzini, P., Gozzo, F., Pelliccia, V., Mai, R., Abdollahi, R.O., Cardinale, F., Sartori, I., Lo Russo, G., Rizzolatti, G., 2018. Motor and emotional behaviours elicited by electrical stimulation of the human cingulate cortex. Brain 1, 1–17.

Cauda, F., Geminiani, G., D'Agata, F., Sacco, K., Duca, S., Bagshaw, A.P., Cavanna, A.E., 2010. Functional connectivity of the posteromedial cortex. PLoS One 5, e13107.

Cavanna, A.E., Trimble, M.R., 2006. The precuneus: a review of its functional anatomy and behavioural correlates. Brain 129, 564–583.

Cha, J., Jo, H.J., Gibson, W.S., Lee, J.M., 2017. Functional organization of the human posterior cingulate cortex, revealed by multiple connectivity-based parcellation methods. Hum. Brain Mapp. 38, 2808–2818.

Christoff, K., Irving, Z.C., Fox, K.C., Spreng, R.N., Andrews-Hanna, J.R., 2016. Mind-wandering as spontaneous thought: a dynamic framework. Nat. Rev. Neurosci. 17, 718–731.

Colby, C., Gattass, R., Olson, C., Gross, C., 1988. Topographical organization of cortical afferents to extrastriate visual area PO in the macaque: a dual tracer study. J. Comp. Neurol. 269, 392–413.

Conner, C.R., Ellmore, T.M., DiSano, M.A., Pieters, T.A., Potter, A.W., Tandon, N., 2011. Anatomic and electro-physiologic connectivity of the language system: a combined DTI-CCEP study. Comput. Biol. Med. 41, 1100–1109.

Daitch, A.L., Parvizi, J., 2018. Spatial and temporal heterogeneity of neural responses in human posteromedial cortex. Proc. Natl. Acad. Sci. U. S. A. 115, 4785–4790.

Dixon, M.L., De La Vega, A., Mills, C., Andrews-Hanna, J., Spreng, R.N., Cole, M.W., Christoff, K., 2018. Heterogeneity within the frontoparietal control network and its relationship to the default and dorsal attention networks. Proc. Natl. Acad. Sci., 201715766.

Donos, C., Maliia, M.D., Mindruta, I., Popa, I., Ene, M., Balanescu, B., Ciurea, A., Barborica, A., 2016. A connectomics approach combining structural and effective connectivity assessed by intracranial electrical stimulation. Neuroimage 132, 344–358.

Emmanuel, P., Wilson Charles, R., Stoll Frederic, M., Faraut Maïlys, C., Michael, P., Céline, A., 2016. Midcingulate motor map and feedback detection: converging data from humans and monkeys.

Enatsu, R., Bulacio, J., Nair, D.R., Bingaman, W., Najm, I., Gonzalez-Martinez, J., 2014. Posterior cingulate epilepsy: clinical and neurophysiological analysis. J. Neurol. Neurosurg. Psychiatry 85, 44–50.

Enatsu, R., Gonzalez-Martinez, J., Bulacio, J., Kubota, Y., Mosher, J., Burgess, R.C., Najm, I., Nair, D.R., 2015. Connections of the limbic network: a corticocortical evoked potentials study. Cortex 62, 20–33.

Entz, L., Toth, E., Keller, C.J., Bickel, S., Groppe, D.M., Fabo, D., Kozak, L.R., Eross, L., Ulbert, I., Mehta, A.D., 2014. Evoked effective connectivity of the human neocortex. Hum. Brain Mapp. 35, 5736–5753.

Fernandez-Ruiz, J., Goltz, H.C., DeSouza, J.F., Vilis, T., Crawford, J.D., 2007. Human parietal "reach region" primarily encodes intrinsic visual direction, not extrinsic movement direction, in a visual motor dissociation task. Cereb. Cortex 17, 2283–2292.

Fox, K.C.R., Foster, B.L., Kucyi, A., Daitch, A.L., Parvizi, J., 2018. Intracranial Electrophysiology of the Human Default Network. Trends Cogn. Sci. 22, 307–324.

Fransson, P., Marrelec, G., 2008. The precuneus/posterior cingulate cortex plays a pivotal role in the default mode network: evidence from a partial correlation network analysis. Neuroimage 42, 1178–1184.

Friston, K.J., 2011. Functional and effective connectivity: a review. Brain Connect 1, 13–36.

Glanz Iljina, O., Derix, J., Kaur, R., Schulze-Bonhage, A., Auer, P., Aertsen, A., Ball, T., 2018. Real-life speech production and perception have a shared premotor-cortical substrate. Sci. Rep. 8, 8898.

Harroud, A., Boucher, O., Tran, T.P.Y., Harris, L., Hall, J., Dubeau, F., Mohamed, I., Bouthillier, A., Nguyen, D.K., 2017. Precuneal epilepsy: clinical features and surgical outcome. Epilepsy Behav. 73, 77–82.

Hoshi, E., Tanji, J., 2007. Distinctions between dorsal and ventral premotor areas: anatomical connectivity and functional properties. Curr. Opin. Neurobiol. 17, 234–242.

Humphreys, G.F., Lambon Ralph, M.A., 2015. Fusion and Fission of Cognitive Functions in the Human Parietal Cortex. Cereb. Cortex 25, 3547–3560.

Hutchison, R.M., Culham, J.C., Flanagan, J.R., Everling, S., Gallivan, J.P., 2015. Functional subdivisions of medial parieto-occipital cortex in humans and nonhuman primates using resting-state fMRI. Neuroimage 116, 10–29.

Johnson, P.B., Ferraina, S., Bianchi, L., Caminiti, R., 1996. Cortical networks for visual reaching: physiological and anatomical organization of frontal and parietal lobe arm regions. Cereb. Cortex 6, 102–119.

Keller, C.J., Bickel, S., Entz, L., Ulbert, I., Milham, M.P., Kelly, C., Mehta, A.D., 2011. Intrinsic functional architecture predicts electrically evoked responses in the human brain. Proc. Natl. Acad. Sci. U. S. A. 108, 10308–10313.

Keller, C.J., Honey, C.J., Entz, L., Bickel, S., Groppe, D.M., Toth, E., Ulbert, I., Lado, F.A., Mehta, A.D., 2014a. Corticocortical evoked potentials reveal projectors and integrators in human brain networks. J. Neurosci. 34, 9152–9163.

Keller, C.J., Honey, C.J., Megevand, P., Entz, L., Ulbert, I., Mehta, A.D., 2014b. Mapping human brain networks with cortico-cortical evoked potentials. Philos. Trans. R. Soc. Lond. B Biol. Sci. 369.

Kobayashi, K., Matsumoto, R., Matsuhashi, M., Usami, K., Shimotake, A., Kunieda, T., Kikuchi, T., Yoshida, K., Mikuni, N., Miyamoto, S., Fukuyama, H., Takahashi, R., Ikeda, A., 2017. High frequency activity overriding cortico-cortical evoked potentials reflects altered excitability in the human epileptic focus. Clin. Neurophysiol. 128, 1673–1681.

Kubota, Y., Enatsu, R., Gonzalez-Martinez, J., Bulacio, J., Mosher, J., Burgess, R.C., Nair, D.R., 2013. In vivo human hippocampal cingulate connectivity: a corticocortical evoked potentials (CCEPs) study. Clin. Neurophysiol. 124, 1547–1556.

Leichnetz, G.R., 2001. Connections of the medial posterior parietal cortex (area 7m) in the monkey. Anat. Rec. 263, 215–236.

Mailo, J., Tang-Wai, R., 2015. Insight into the precuneus: a novel seizure semiology in a child with epilepsy arising from the right posterior precuneus. Epileptic Disord. 17, 321–327.

Margulies, D.S., Vincent, J.L., Kelly, C., Lohmann, G., Uddin, L.Q., Biswal, B.B., Vill-

ringer, A., Castellanos, F.X., Milham, M.P., Petrides, M., 2009. Precuneus shares intrinsic functional architecture in humans and monkeys. Proc. Natl. Acad. Sci. U. S. A. 106, 20069–20074.

Mars, R.B., Jbabdi, S., Sallet, J., O'Reilly, J.X., Croxson, P.L., Olivier, E., Noonan, M.P., Bergmann, C., Mitchell, A.S., Baxter, M.G., Behrens, T.E., Johansen-Berg, H., Tomassini, V., Miller, K.L., Rushworth, M.F., 2011. Diffusion-weighted imaging tractography-based parcellation of the human parietal cortex and comparison with human and macaque resting-state functional connectivity. J. Neurosci. 31, 4087–4100.

Matelli, M., Govoni, P., Galletti, C., Kutz, D.F., Luppino, G., 1998. Superior area 6 afferents from the superior parietal lobule in the macaque monkey. J. Comp. Neurol. 402, 327–352.

Matsumoto, R., Imamura, H., Inouchi, M., Nakagawa, T., Yokoyama, Y., Matsuhashi, M., Mikuni, N., Miyamoto, S., Fukuyama, H., Takahashi, R., Ikeda, A., 2011. Left anterior temporal cortex actively engages in speech perception: a direct cortical stimulation study. Neuropsychologia 49, 1350–1354.

Matsumoto, R., Kunieda, T., Nair, D., 2017. Single pulse electrical stimulation to probe functional and pathological connectivity in epilepsy. Seizure 44, 27–36.

Matsumoto, R., Nair, D.R., Ikeda, A., Fumuro, T., Lapresto, E., Mikuni, N., Bingaman, W., Miyamoto, S., Fukuyama, H., Takahashi, R., Najm, I., Shibasaki, H., Luders, H.O., 2012. Parieto-frontal network in humans studied by cortico-cortical evoked potential. Hum. Brain Mapp. 33, 2856–2872.

Matsumoto, R., Nair, D.R., LaPresto, E., Bingaman, W., Shibasaki, H., Luders, H.O., 2007. Functional connectivity in human cortical motor system: a cortico-cortical evoked potential study. Brain 130, 181–197.

Matsumoto, R., Nair, D.R., LaPresto, E., Najm, I., Bingaman, W., Shibasaki, H., Luders, H.O., 2004. Functional connectivity in the human language system: a cortico–cortical evoked potential study. Brain 127, 2316–2330.

Nakae, T., Matsumoto, R., Kunieda, T., Arakawa, Y., Kobayashi, K., Shimotake, A., Yamao, Y., Kikuchi, T., Aso, T., Matsuhashi, M., Yoshida, K., Ikeda, A., Takahashi, R., Lambon Ralph, M.A., Miyamoto, S., 2020. Connectivity Gradient in the Human Left Inferior Frontal Gyrus: intraoperative Cortico-Cortical Evoked Potential Study. Cereb. Cortex 30, 4633–4650.

Pandya, D., Van Hoesen, G., Mesulam, M.-.M., 1981. Efferent connections of the cingulate gyrus in the rhesus monkey. Exp. Brain Res. 42, 319–330.

Parvizi, J., Van Hoesen, G.W., Buckwalter, J., Damasio, A., 2006. Neural connections of the posteromedial cortex in the macaque. Proc. Natl. Acad. Sci. U. S. A. 103, 1563–1568.

Parvizi, J., Braga, R.M., Kucyi, A., Veit, M.J., Pinheiro-Chagas, P., Perry, C., Sava-Segal, C., Zeineh, M., van Staalduinen, E.K., Henderson, J.M., Markert, M., 2021. Altered sense of self during seizures in the posteromedial cortex. Proc. Natl Acad. Sci. U S A 118.

Passarelli, L., Rosa, M.G., Gamberini, M., Bakola, S., Burman, K.J., Fattori, P., Galletti, C., 2011. Cortical connections of area V6Av in the macaque: a visual-input node to the eye/hand coordination system. J. Neurosci. 31, 1790–1801.

Paulk, A.C., Zelmann, R., Crocker, B., Widge, A.S., Dougherty, D.D., Eskandar, E.N., Weisholtz, D.S., Richardson, R.M., Cosgrove, G.R., Williams, Z.M., Cash, S.S., 2022. Local and distant cortical responses to single pulse intracranial stimulation in the human brain are differentially modulated by specific stimulation parameters. Brain Stimul. 15, 491–508.

Prime, D., Rowlands, D., O'Keefe, S., Dionisio, S., 2018. Considerations in performing and analyzing the responses of cortico-cortical evoked potentials in stereo-EEG. Epilepsia 59, 16–26.

Raichle, M.E., 2015. The brain's default mode network. Annu. Rev. Neurosci. 38, 433–447.

Raichle, M.E., MacLeod, A.M., Snyder, A.Z., Powers, W.J., Gusnard, D.A., Shulman, G.L., 2001. A default mode of brain function. Proc. Natl. Acad. Sci. 98, 676–682.

Saeki, K., Saito, Y., Sugai, K., Nakagawa, E., Komaki, H., Sakuma, H., Sasaki, M., Kaneko, Y., 2009. Startle epilepsy associated with gait-induced seizures: pathomechanism analysis using EEG, MEG, and PET studies. Epilepsia 50, 1274–1279.

Sugiura, M., Shah, N.J., Zilles, K., Fink, G.R., 2005. Cortical representations of personally familiar objects and places: functional organization of the human posterior cingulate cortex. J. Cogn. Neurosci. 17, 183–198.

Takahashi, N., Kawamura, M., Shiota, J., Kasahata, N., Hirayama, K., 1997. Pure topographic disorientation due to right retrosplenial lesion. Neurology 49, 464–469.

Toga, A.W., 2015. Brain mapping: An encyclopedic Reference. Academic Press.

Trebaul, L., Deman, P., Tuyisenge, V., Jedynak, M., Hugues, E., Rudrauf, D., Bhattacharjee, M., Tadel, F., Chanteloup-Foret, B., Saubat, C., Reyes Mejia, G.C., Adam, C., Nica, A., Pail, M., Dubeau, F., Rheims, S., Trebuchon, A., Wang, H., Liu, S., Blauwblomme, T., Garces, M., De Palma, L., Valentin, A., Metsahonkala, E.L., Petrescu, A.M., Landre, E., Szurhaj, W., Hirsch, E., Valton, L., Rocamora, R., Schulze-Bonhage, A., Mindruta, I., Francione, S., Maillard, L., Taussig, D., Kahane, P., David, O., 2018. Probabilistic functional tractography of the human cortex revisited. Neuroimage 181, 414–429.

Umeoka, S., Baba, K., Terada, K., Matsuda, K., Tottori, T., Usui, N., Usui, K., Nakamura, F., Inoue, Y., Fujiwara, T., Mihara, T., 2007. Bilateral symmetric tonic posturing suggesting propagation to the supplementary motor area in a patient with precuneate cortical dysplasia. Epileptic Disord. 9, 443–448.

Utevsky, A.V., Smith, D.V., Huettel, S.A., 2014. Precuneus is a functional core of the default-mode network. J. Neurosci. 34, 932–940.

Veit, M.J., Kucyi, A., Hu, W., Zhang, C., Zhao, B., Guo, Z., Yang, B., Sava-Segal, C., Perry, C., Zhang, J., Zhang, K., Parvizi, J., 2021. Temporal order of signal propagation within and across intrinsic brain networks. Proc. Natl Acad. Sci. U S A 118.

Vogt, B., 2009. Cingulate Neurobiology and Disease. Oxford University Press.

Vogt, B.A., 2016. Midcingulate cortex: structure, connections, homologies, functions and diseases. J. Chem. Neuroanat. 74, 28–46.

Vogt, B.A., Nimchinsky, E.A., Vogt, L.J., Hof, P.R., 1995. Human cingulate cortex: surface features, flat maps, and cytoarchitecture. J. Comp. Neurol. 359, 490–506.

Vogt, B.A., Pandya, D.N., 1987. Cingulate cortex of the rhesus monkey: II. Cortical afferents. J. Comp. Neurol. 262, 271–289.

Vogt, B.A., Vogt, L., Laureys, S., 2006. Cytology and functionally correlated circuits of human posterior cingulate areas. Neuroimage 29, 452–466.

Wang, J., Yang, Y., Fan, L., Xu, J., Li, C., Liu, Y., Fox, P.T., Eickhoff, S.B., Yu, C., Jiang, T., 2015. Convergent functional architecture of the superior parietal lobule unraveled with multimodal neuroimaging approaches. Hum. Brain Mapp. 36, 238–257.

Wiest, G., Zimprich, F., Prayer, D., Czech, T., Serles, W., Baumgartner, C., 2004. Vestibular processing in human paramedian precuneus as shown by electrical cortical stimulation. Neurology 62, 473–475.

Yarkoni, T., Poldrack, R.A., Nichols, T.E., Van Essen, D.C., Wager, T.D., 2011. Large-scale automated synthesis of human functional neuroimaging data. Nat. Methods 8, 665–670.

Yeo, B.T., Krienen, F.M., Sepulcre, J., Sabuncu, M.R., Lashkari, D., Hollinshead, M., Roffman, J.L., Smoller, J.W., Zollei, L., Polimeni, J.R., Fischl, B., Liu, H., Buckner, R.L., 2011. The organization of the human cerebral cortex estimated by intrinsic functional connectivity. J. Neurophysiol. 106, 1125–1165.

Yu, C., Zhou, Y., Liu, Y., Jiang, T., Dong, H., Zhang, Y., Walter, M., 2011. Functional segregation of the human cingulate cortex is confirmed by functional connectivity based neuroanatomical parcellation. Neuroimage 54, 2571–2581.

Zhang, S., Li, C.S., 2012. Functional connectivity mapping of the human precuneus by resting state fMRI. Neuroimage 59, 3548–3562.

Zhang, Y., Fan, L., Zhang, Y., Wang, J., Zhu, M., Zhang, Y., Yu, C., Jiang, T., 2014. Connectivity-based parcellation of the human posteromedial cortex. Cereb. Cortex 24, 719–727.